IRAQI JOURNAL OF MATERIALS
Volume (4) Issue (4) October-December 2025, pp. 145-152

Effects of Partial Oxygen Content on Crystalline Structure and Surface Topography of Nanostructured Al_2O_3 Thin Films Prepared by DC Reactive Sputtering Technique

Haneen H. Shaaban, Mohammed A. Hameed

Department of Physics, College of Science, University of Baghdad, Baghdad, IRAQ

Abstract
Aluminum oxide thin films were prepared by dc reactive sputtering technique using different mixing ratios of argon and oxygen gases (90:10, 70:30, 50:50, 30:70, and 10:90). These films were characterized to introduce their crystalline structures, surface morphology, and elemental composition. A progressive transition occurs from a predominantly amorphous to a highly crystalline Al_2O_3 film as the oxygen content in the Ar:O_2 gas mixture is increased. Increasing the oxygen content leads to a progressive decrease in surface roughness, resulting in smoother and more uniform films with finer granular features. The oxygen-rich environments yield the smoothest surfaces, while argon-rich environments result in significantly rougher surfaces. These findings are critical for optimizing the sputtering process to achieve desired surface properties for various applications, as surface roughness profoundly impacts adhesion, optical properties, and device performance.

Keywords: Aluminum oxide; DC sputtering; Structural characteristics; Gas mixtures
Received: 11 June 2025; **Revised:** 27 July 2025; **Accepted:** 3 August 2025; **Published:** 1 October 2025

1. Introduction

The composition of the gas mixture in DC reactive sputtering exerts a profound influence on the inherent structural attributes of nanostructured metal oxide thin films, directly impacting aspects such as their crystalline arrangement, elemental proportionality, particulate dimensions, outward appearance, and concentration of imperfections [1,2]. Within this sputtering process, a pure metal target is subjected to bombardment within an environment comprising both an inert gas, typically argon (Ar), and a reactive gas, such as oxygen (O_2) for oxide film formation [3]. The precise proportion of these gases directly modulates the intricate chemical reactions within the plasma, the efficiency with which material is ejected from the target, and the specific chemical interactions occurring both on the target's surface and on the developing film [4,5].

When the reactive gas flow rate is kept low, signifying a high ratio of Ar to reactive gas, the sputtering process operates in what is termed a metallic mode. In this state, the target's surface predominantly retains its metallic nature, facilitating a rapid ejection of metal atoms. The reactive gas primarily engages in chemical reactions with these dislodged metal atoms either within the plasma itself or upon their arrival at the substrate [6]. This typically results in the formation of films characterized by high density, well-defined crystalline structures, and a generally consistent elemental composition, owing to the abundant supply of metal atoms available for reaction [7]. However, an insufficient supply of reactive gas can lead to the formation of oxygen vacancies or an oxide phase with an imbalanced elemental ratio, which can compromise the film's intended functional properties. For instance, in materials like transparent conducting oxides, while oxygen vacancies can facilitate electrical conductivity, an excessive number can paradoxically diminish transparency or stability [8-10].

As the reactive gas flow rate progressively increases, the sputtering process undergoes a transformation, transitioning from the metallic mode through a transition mode and ultimately culminating in a poisoned mode [13]. In the intermediate "transition mode," the target's surface begins to be partially coated by the reactive gas, forming a thin layer of the compound (e.g., metal oxide). This surface passivation detrimentally affects the rate at which metal atoms are ejected because the newly formed compound layer exhibits a lower sputtering yield compared to the pure metal. Consequently, the film growth rate diminishes, and the plasma characteristics undergo alteration due to changes in the emission of secondary electrons from the now-passivated target [14-16]. This operational regime is frequently associated with unstable sputtering conditions, presenting challenges in achieving consistent and predictable film properties [17]. Nevertheless, some researchers intentionally operate within this

region to precisely refine specific structural properties, as it offers a delicate equilibrium between a metallic and a fully oxidized target state [18,19].

In the poisoned mode, characterized by a high reactive gas flow rate and a low Ar-to-reactive gas ratio, the target's surface becomes entirely covered by the reactive compound. This results in a substantial reduction in the sputtering yield, leading to significantly slower deposition rates. While this mode ensures the formation of films that are highly stoichiometric and thoroughly oxidized, it can also lead to increased porosity, a reduction in film density, and a diminished level of crystallinity due to the restricted mobility of atoms on the growing surface at these slower deposition rates [20-22]. An excessive amount of reactive gas can also promote the formation of undesirable phases or an increased incorporation of impurities [23,24]. Furthermore, the effects of ion bombardment from the plasma can be modified; a higher concentration of reactive gas can cause a shift in the plasma potential, thereby influencing the kinetic energy of ions striking the substrate, which in turn impacts the film's compaction, internal stresses, and crystallographic orientation [25-27].

Ultimately, the gas mixing ratio plays a pivotal role in determining the average distance a sputtered particle or a reactive gas molecule can travel before colliding with another particle within the plasma. This, in turn, critically influences the energy and directional distribution of the species that ultimately arrive at the substrate, significantly shaping the film's overall morphology and textural characteristics. For example, an elevated partial pressure of the reactive gas can intensify gas-phase scattering, leading to a reduction in the kinetic energy of the arriving species and potentially resulting in the formation of more porous films [29-32]. Conversely, an optimized kinetic energy can facilitate surface diffusion, promoting the growth of denser films. Therefore, meticulous regulation of the gas mixing ratio is absolutely essential for customizing the desired structural characteristics, enhancing the physical and chemical attributes, and guaranteeing the consistent production of high-performance nanostructured metal oxide thin films for a broad spectrum of applications across electronics, optics, and sensor technologies [33-36].

Aluminum oxide (Al_2O_3) thin films are a class of widely utilized materials due to their exceptional combination of physical, chemical, and electrical properties, making them indispensable in various scientific and technological applications [37]. These properties stem from their robust atomic structure, characterized by strong ionic-covalent bonds between aluminum and oxygen atoms. Structurally, Al_2O_3 can exist in several crystalline phases, including amorphous, γ, δ, θ, and the thermodynamically most stable α-Al_2O_3 (corundum), each exhibiting slightly different properties depending on the deposition parameters and post-deposition treatments [38,39]. Key properties include high dielectric strength (typically >10 MV/cm), which is crucial for insulating layers in microelectronics, and a relatively high dielectric constant (≈9−10), beneficial for capacitance applications. They possess excellent thermal stability, with high melting points (over 2000°C), making them resistant to extreme temperatures, a vital characteristic for protective coatings and high-temperature devices [40]. Furthermore, Al_2O_3 films exhibit remarkable chemical inertness and corrosion resistance, providing effective barriers against harsh environments and preventing degradation of underlying materials. Their optical transparency across a broad spectrum, from ultraviolet to infrared, coupled with a high refractive index (≈1.6−1.8), makes them valuable for optical coatings, anti-reflection layers, and dielectric mirrors [41]. Mechanically, Al_2O_3 thin films are known for their high hardness and wear resistance, often employed as protective layers on tools and components subjected to friction [42].

The aim of this work is to introduce the effects of partial gas content of oxygen in the gas mixture on the crystalline structure and surface topography of nanostructured Al_2O_3 thin films by dc reactive sputtering technique.

2. Experimental Part

This work utilized a custom-built DC reactive magnetron sputtering system, depicted schematically in Fig. (1), to produce aluminum oxide (Al_2O_3) thin films. A high-purity (99.99%) aluminum sheet served as the sputtering target, used in an oxygen atmosphere to deposit Al2O3 films onto glass substrates. Prior to deposition, both the targets and glass substrates underwent thorough cleaning and drying. The target was meticulously positioned on the cathode, and sputtering plasma was generated by an electrical discharge of argon, powered by a high-voltage DC supply (up to 5kV). The technique involved gas mixtures of argon and oxygen with various mixing ratios (10:90, 30:70, 50:50, 70:30, 90:10). The deposition chamber was initially evacuated to 0.001 Torr, and the process was conducted at room temperature with a discharge voltage of 650-700 V and a discharge current of 25 mA. Deposition times for all samples were fixed at 30, 45, 60, 90, and 120 minutes, with an inter-electrode distance of 4 cm. The optimal discharge current was determined by plasma discharge stability. The gas mixture pressure

 ISSN (print) 2958-8960 (online) 3006-6042 Printed in IRAQ

was maintained at approximately 0.15 mbar. Figure (1) details the stainless steel deposition chamber, featuring eight observation windows, fixed anode and cathode connected externally to the DC power supply, a gas mixture inlet from an external mixer, and an outlet for evacuation via a rotary pump. Applied voltage and discharge current were continuously monitored by a voltmeter and ammeter, respectively. Gas mixture flow rate was precisely controllable, and chamber temperature was measured by a precision thermometer. Argon and oxygen were supplied from gas cylinders to the mixer, with ratios controlled by fine needle valves. Both electrodes incorporated a water-cooling system via internal channels. Further specifics on this sputtering system are available in references [24-27].

Film thickness was determined using optical interferometry, a method based on coherent light beam interference reflected from the film surface and substrate bottom, with an error rate of about 3%. A 630 nm diode laser served as the light source. Film thickness (d) was calculated using the formula: $d=(x\lambda/2\Delta x)$, where x is fringe width, Δx is the distance between two fringes, and λ is the laser wavelength [28,29]. Prepared samples underwent comprehensive characterization including X-ray diffraction (XRD), scanning electron microscopy (SEM), energy dispersive X-ray spectroscopy (EDS), atomic force microscopy (AFM), and thickness measurements.

3. Results and Discussion

Figure (1) illustrates the relationship between the thickness of Al_2O_3 thin films and their deposition time, using the DC reactive sputtering technique. Initially, as the deposition time increases from 30 minutes to 45 minutes, the film thickness decreases from approximately 330 nm to 300 nm, suggesting a potential non-linear or complex growth mechanism. A more significant decrease in film thickness is observed as the deposition time extends to 60 minutes, where the thickness drops to around 210 nm. This unexpected reduction in thickness with increasing deposition time might indicate effects like increased re-sputtering, a shift in deposition regime, or changes in film density over longer sputtering durations. However, for deposition times beyond 60 minutes, up to 90 minutes, the film thickness begins to slightly increase again, reaching about 250 nm. This non-monotonic behavior highlights that the deposition rate is not constant and is influenced by sputtering time, possibly due to target poisoning, substrate heating, or other dynamic processes inherent in DC reactive sputtering.

The X-ray diffraction (XRD) patterns in Fig. (2) illustrate the structural evolution of Al_2O_3 thin films prepared by DC reactive sputtering, as a function of varying Ar:O_2) gas mixing ratios: 90:10 (black), 70:30 (red), 50:50 (green), 30:70 (cyan), and 10:90 (orange). Each spectrum is shifted vertically for clarity. The analysis of these patterns reveals a significant impact of the Ar:O_2 ratio on the crystallinity and phase formation of the Al_2O_3 films.

The gas mixture of 90:10 represents the highest argon and lowest oxygen content, the XRD pattern primarily shows a broad, amorphous hump centered around $2\theta \approx 20-30^\circ$. This indicates that the film deposited under such oxygen-deficient conditions is largely amorphous or nanocrystalline, with very limited long-range order. The presence of a few very weak, broad peaks at higher 2θ values suggests the initial formation of some minute crystalline phases, but their low intensity and broadness confirm a predominantly amorphous structure. The insufficient oxygen supply hinders the proper formation of crystalline Al_2O_3 phases, often leading to a non-stoichiometric or poorly ordered structure. As the oxygen content is increased to 30% (i.e., mixing ratio of 70:30), the pattern begins to show clearer, albeit still broad, diffraction peaks superimposed on an amorphous background. Peaks start to emerge around $2\theta \approx 35^\circ$, 45°, 60°, and 67°. While these peaks are not perfectly sharp, their appearance signifies a notable increase in the degree of crystallinity compared to the 90:10 ratio. This suggests that a greater supply of oxygen facilitates the nucleation and growth of crystalline Al_2O_3 phases. These peaks likely correspond to various planes of $\gamma-Al_2O_3$ or other transition alumina phases, which are commonly observed in sputtered films.

With further increasing the oxygen content to 50% (i.e., mixing ratio of 50:50), the XRD pattern shows a more pronounced increase in the intensity and sharpness of the crystalline peaks. The amorphous hump diminishes significantly, and the crystalline peaks become more distinct and well-defined, indicating a higher volume fraction of crystalline Al_2O_3. This ratio appears to be highly effective in promoting crystallization, possibly due to an optimized balance between sputtering yield of aluminum and the reactive oxidation process. The enhanced peak intensity suggests larger crystallite sizes or a higher degree of crystalline order. Using a mixing ratio of 30:70, where oxygen is dominant, the crystalline peaks become even sharper and more intense, particularly at the positions previously identified. The baseline is relatively flat, signifying a largely crystalline film with minimal amorphous content. The increased peak sharpness suggests further growth of crystallites and improved crystallinity. This implies that a sufficient surplus of oxygen is crucial for achieving well-crystallized Al_2O_3 films under

 ISSN (print) 2958-8960 (online) 3006-6042 Printed in IRAQ

these sputtering conditions. Finally, at the highest oxygen content of 90% (i.e., mixing ratio of 10:90), the XRD pattern exhibits the sharpest and most intense diffraction peaks among all samples. The peaks are highly resolved and prominent, indicating the highest degree of crystallinity and possibly the largest crystallite size. The absence of a significant amorphous hump further confirms the highly crystalline nature of the film. The increased oxygen partial pressure ensures complete oxidation and provides ample oxygen species for the formation of stable crystalline phases, such as γ−Al_2O_3 or even a transition towards α−Al_2O_3 if sufficient energy is supplied during deposition. The XRD analysis clearly demonstrates a progressive transition from a predominantly amorphous to a highly crystalline Al_2O_3 film as the oxygen content in the Ar:O_2 sputtering gas mixture increases. Low oxygen content leads to amorphous films, while increasing oxygen promotes the formation and growth of crystalline Al_2O_3 phases, with the 10:90 Ar:O_2 ratio yielding the most crystalline films. This highlights the critical role of oxygen partial pressure in controlling the structural properties of sputtered Al_2O_3 films.

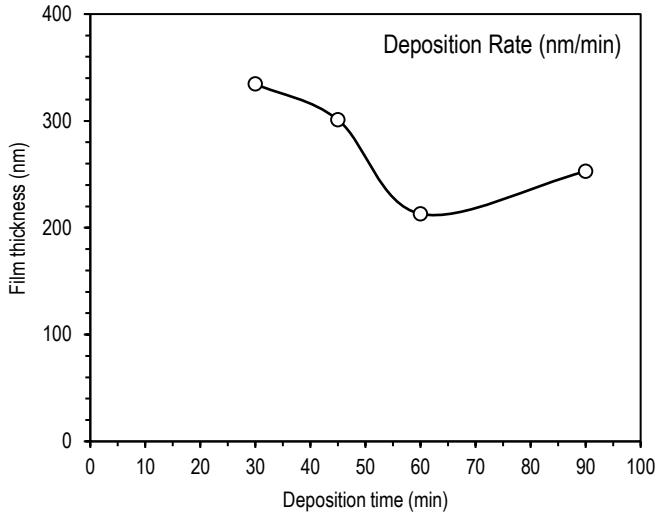

Fig. (1) Deposition rate of the Al_2O_3 thin films prepared in this work

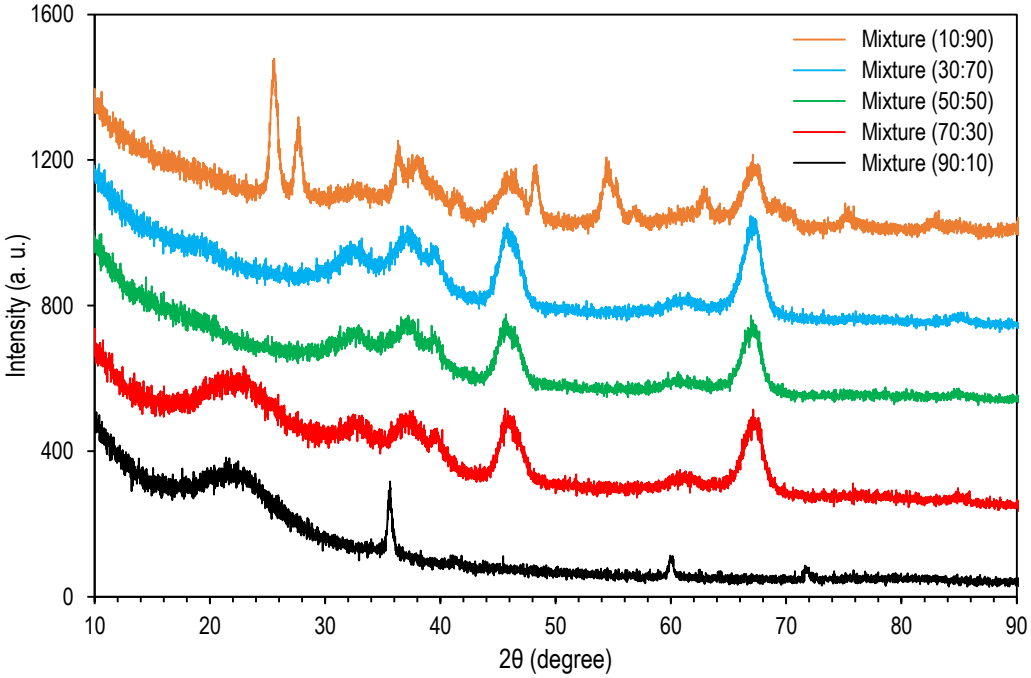

Fig. (2) XRD patterns of the Al_2O_3 thin films prepared in this work

The 2D and 3D AFM images in Fig. (3) offers a detailed look into the surface morphology of Al_2O_3 thin films prepared in this work. The color scales (representing height variations) provided alongside

ISSN (print) 2958-8960 (online) 3006-6042 Printed in IRAQ

each image are crucial for a quantitative understanding of the surface roughness and topographical features. A comparative analysis of these images reveals how the Ar:O_2 ratio significantly impacts the nanoscale roughness, grain size, and overall homogeneity of the deposited Al_2O_3 films. At a first glance, all images depict a granular surface, which is typical for thin films grown by sputtering. However, the uniformity, size of the apparent grains, and the extent of peak-to-valley variations differ considerably across the samples. The color scale, which maps height, is a direct indicator of the film's roughness. A wider range in the color scale suggests a rougher surface with greater topographical variations, while a narrower range indicates a smoother film.

For the sample prepared using gas mixing ratio of 90:10, the surface displays the roughest morphology among all the samples. Large, irregularly shaped agglomerates and distinct peaks and valleys are clearly visible. The overall texture is highly non-uniform. The height scale for this image extends from approximately 0 to 25 nm, indicating the largest vertical variations and thus the highest surface roughness. The very limited oxygen supply under these conditions severely hinders complete oxidation, leading to the formation of poorly crystalline or oxygen-deficient AlO_x phases, which tend to grow in larger, less organized structures. This results in a rough, heterogeneous film surface. For the sample prepared using gas mixing ratio of 70:30, the surface exhibits a more distinct granular structure with larger and more irregularly shaped features compared to the oxygen-rich samples. The height variations are visibly greater. The height scale for this image spans from approximately 0 to 18 nm, indicating a higher degree of surface roughness. The higher argon content likely leads to a more energetic sputtering process and potentially less complete oxidation of the aluminum target and deposited film. This can result in the formation of larger particles, voids, or non-uniform growth, contributing to increased surface roughness. For the sample prepared using gas mixing ratio of 50:50, which corresponds to an intermediate gas mixing ratio, the surface morphology shows a noticeable change compared to the oxygen-rich samples. While still relatively uniform, the granular features appear slightly larger and more pronounced, and the overall texture seems coarser. The height scale for this image is approximately 0 to 12 nm, indicating a moderate increase in surface roughness compared to the 10:90 and 30:70 ratios. This might suggest that at this balanced ratio, there's a slight increase in grain size or a change in growth mode that leads to greater topographical variations. This could be due to a different balance between the sputtering rate and the oxidation rate, potentially promoting more significant grain growth. For the sample prepared using gas mixing ratio of 30:70, this sample also falls under oxygen-rich conditions. Visually, the surface still appears very smooth and uniform. The height scale for this image is also quite narrow, ranging from approximately 0 to 8 nm. This suggests that even with a slightly reduced oxygen flow, the sputtering conditions are still conducive to form smooth Al_2O_3 films with low roughness. The ample oxygen supply continues to promote efficient oxidation and fine grain growth, contributing to surface regularity. For the sample prepared using gas mixing ratio of 10:90, the surface appears relatively smooth and uniform, characterized by very fine, densely packed granular features. The height scale for this image ranges approximately from 0 to 8 nm, indicating small vertical variations. The RMS roughness would likely be low for this sample. The high oxygen concentration facilitates the complete oxidation of sputtered aluminum atoms, leading to the formation of small, well-defined Al_2O_3 nanocrystallites and a dense, homogeneous film structure. This often translates to a low surface roughness, making it desirable for applications requiring highly smooth surfaces.

1. Conclusions

In concluding remarks, a progressive transition occurs from a predominantly amorphous to a highly crystalline Al_2O_3 film as the oxygen content in the Ar:O_2 gas mixture is increased. Low oxygen content leads to amorphous films, while increasing O_2 promotes the formation and growth of crystalline Al_2O_3 phases, with the 10:90 ratio yielding the most crystalline films. Increasing the oxygen content leads to a progressive decrease in surface roughness, resulting in smoother and more uniform films with finer granular features. The oxygen-rich environments yield the smoothest surfaces, characterized by small, densely packed grains and minimal height variations. Conversely, argon-rich environments result in significantly rougher surfaces with larger, more irregular granular features and greater topographical variations. These findings are critical for optimizing the sputtering process to achieve desired surface properties for various applications, as surface roughness profoundly impacts adhesion, optical properties, and device performance.

ISSN (print) 2958-8960 (online) 3006-6042 Printed in IRAQ

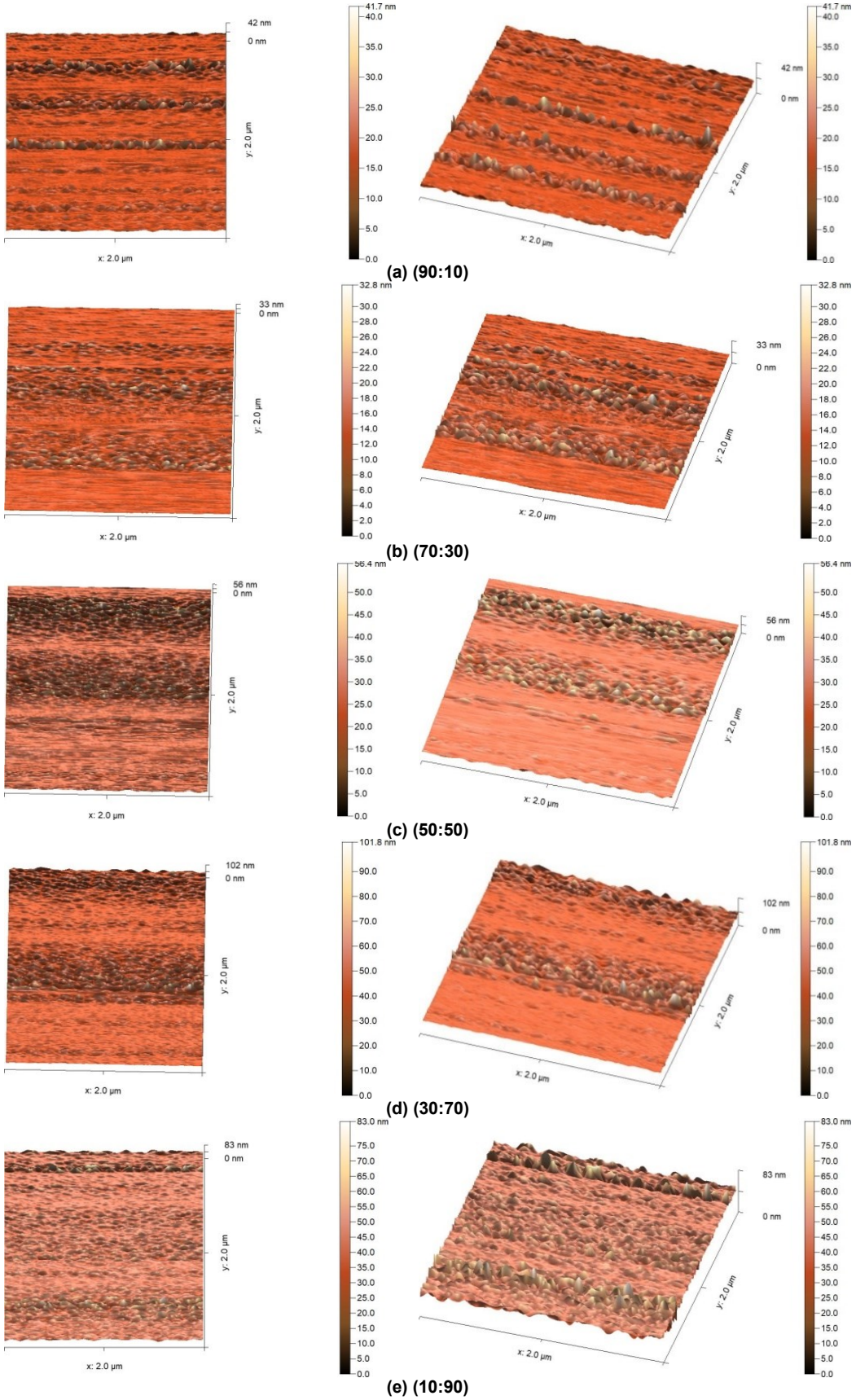

Fig. (3) 2D and 3D AFM images of the Al_2O_3 thin films prepared in this work

References

[1] P.M. Martin, **"Introduction to Surface Engineering and Functionally Engineered Materials"**, Ch. 6, John Wiley & Sons (NJ, 2011), p. 339.
[2] A.S. Reddy, H.-H. Park and V.S. Reddy, "Effect of sputtering power on the physical properties of dc magnetron sputtered copper oxide thin films", *Mater. Chem. Phys.*, 110(2-3) (2008) 397-401.
[3] K. Seshan, **"Handbook of Thin Film Deposition: Techniques, Processes, and Technologies"**, 3rd ed., Ch. 4, William Andrew (Amsterdam, 2012).
[4] D. Mattox, **"Handbook of Physical Vapor Deposition (PVD) Processing"**, 2nd ed., Ch. 7, William Andrew, (Amsterdam, 2010).
[5] F.J. Kadhim et al., "Fabrication of UV Photodetector from Nickel Oxide Nanoparticles Deposited on Silicon Substrate by Closed-Field Unbalanced Dual Magnetron Sputtering Techniques", *Opt. Quantum Electron.*, 47(12) (2015) 3805-3813.
[6] D.A. Taher and M.A. Hameed, "Employment of Silicon Nitride Films Prepared by DC Reactive Sputtering Technique for Ion Release Applications", *Iraqi J. Phys.*, 21(3) (2023) 33-40.
[7] A. V. Tumarkin et al., "Preparation of alumina thin films by reactive modulated pulsed power magnetron sputtering with millisecond pulses", *Coatings*, 14(1) (2024) 82.
[8] M.K. Khalaf et al., "Fabrication and Characterization of UV Photodetectors Based on Silicon Nitride Nanostructures Prepared by Magnetron Sputtering", *Proc. IMechE, Part N, J. Nanomater. Nanoeng. Nanosys.*, 230(1) (2016) 32-36.
[9] C. Otero et al., "Optoelectronic Response of Multilayer CuO/NiO Nanostructures Fabricated with Different Particle Size Ranges", *Iraqi J. Appl. Phys. Lett.*, 8(1) (2025) 29-32.
[10] M.A. Hameed and Z.M. Jabbar, "Preparation and Characterization of Silicon Dioxide Nanostructures by DC Reactive Closed-Field Unbalanced Magnetron Sputtering", *Iraqi J. Appl. Phys.*, 12(4) (2016) 13-18.
[11] K.A. Aadim, "Control the deposition uniformity using ring cathode by DC discharge technique", *Iraqi J. Phys.*, 15(32) (2017) 57-60.
[12] O.A. Hammadi, "Nanostructured CdSnSe Thin Films Prepared by DC Plasma Sputtering of Thermally Casted Targets", *Iraqi J. Appl. Phys.*, 14(4) (2018) 33-36.
[13] R.A. Anaee et al., "Alumina Nanoparticle/Polypyrrole Coating for Carbon Steel Protection in Simulated Soil Solution", *Eng. Tech. J.*, 35(9A) (2017) 943-949.
[14] M. Said et al., "Microwave hybrid heating for lead-free solder: A review", *J. Mater. Res. Technol.,* 26 (2023) 6220-6243.
[15] F.J. Al-Maliki et al., "Optimization of Rutile/Anatase Ratio in Titanium Dioxide Nanostructures prepared by DC Magnetron Sputtering Technique", *Iraqi J. Sci.*, 60(special issue) (2019) 91-98.
[16] B.K. Nasser and M.A. Hameed, "Structural Characteristics of Silicon Nitride Nanostructures Synthesized by DC Reactive Magnetron Sputtering", *Iraqi J. Appl. Phys.*, 15(4) (2019) 33-36.
[17] F.J. Al-Maliki and E.A. Al-Oubidy, "Effect of gas mixing ratio on structural characteristics of titanium dioxide nanostructures synthesized by DC reactive magnetron sputtering", *Physica B: Cond. Matter*, 555 (2019) 18-20
[18] S.H. Faisal and M.A. Hameed, "Heterojunction Solar Cell Based on Highly-Pure Nanopowders Prepared by DC Reactive Magnetron Sputtering", *Iraqi J. Appl. Phys.*, 16(3) (2020) 27-32.
[19] S.U. Ilyasa, R. Pendyalaa, and N. Marneni, "Stability and Agglomeration of Alumina Nanoparticles in Ethanol-Water Mixtures", *Procedia Eng.*, 148 (2016) 290-297.
[20] R.H. Turki and M.A. Hameed, "Spectral and Electrical Characteristics of Nanostructured NiO/TiO_2 Heterojunction Fabricated by DC Reactive Magnetron Sputtering", *Iraqi J. Appl. Phys.*, 16(3) (2020) 39-42.
[21] K.A. Al-Hamdani, "Current–voltage and capacitance-voltage characteristics of Se/Si heterojunction prepared by DC planar magnetron sputtering technique", *Iraqi J. Phys.*, 8(13) (2010) 97-100.
[22] M.K. Khalaf et al., "Operation Characteristics of a Closed-Field Unbalanced Dual-Magnetrons Plasma Sputtering System", *Bulg. J. Phys.*, 41(1) (2014) 24-33.
[23] M.A. Hameed et al., "Characterization of Multilayer Highly-Pure Metal Oxide Structures Prepared by DC Reactive Magnetron Sputtering Technique", *Iraqi J. Appl. Phys.*, 16(4) (2020) 25-30
[24] Y. Zhang et al., "A review paper on effect of the welding process of ceramics and metals", *J. Mater. Res. Technol.*, 9(6) (2020) 16214-16236.
[25] A.N. Munif and F.J. Kadhim, "Structural Characteristics and Photocatalytic activity of TiO2/Si3N4 nanocomposite synthesized via plasma sputtering technique", *Iraqi J. Phys.*, 22(4) (2024) 99-106.
[26] E. Kianfar and V. Cao, "Polymeric membranes on base of PolyMethyl methacrylate for air separation: a review", *J. Mater. Res. Technol.*, 10 (2021) 1437-1461.
[27] N.A.H. Hashim and F.J. Kadhim, "Structural and Optical Characteristics of Co_3O_4 Nanostructures Prepared by DC Reactive Magnetron Sputtering", *Iraqi J. Appl. Phys.*, 18(4) (2022) 31-36.
[28] A.Y. Bahlool, "Temperature-Dependent Optoelectronic Characteristics of p-SnO_2/n-Si Heterojunction Structures", *Iraqi J. Appl. Phys. Lett.*, 7(1) (2024) 23-26.
[29] A.M. Hameed and M.A. Hameed, "Spectroscopic characteristics of highly pure metal oxide nanostructures prepared by DC reactive magnetron sputtering technique", *Emerg. Mater.*, 6 (2022) 627-633.
[30] D.A. Taher and M.A. Hameed, "Spectroscopic Characteristics of Silicon Nitride Thin Films Prepared by DC Reactive Sputtering Using Silicon targets with Different Types of Conductivity", *Iraqi J. Appl. Phys.*, 19(4A) (2023) 73-76.
[31] M.S. Edan, "Copper Nitride Nanostructures Prepared by Reactive Plasma Sputtering Technique", *Iraqi J. Mater.*, 4(1) (2025) 31-36.
[32] D.A. Taher and M.A. Hameed, "Structural and Hardness Characteristics of Silicon Nitride Thin Films Deposited on Metallic Substrates by DC Reactive Sputtering Technique", *Silicon*, 15 (2023) 7855-7864.
[33] M.A. Hameed et al., "Characterization of Multilayer Highly-Pure Metal Oxide Structures Prepared by DC Reactive Magnetron Sputtering", *Iraqi J. Mater.*, 3(4) (2024) 1-8.
[34] M.A. Hameed and Z.M. Jabbar, "Optimization of Preparation Conditions to Control Structural Characteristics of Silicon Dioxide Nanostructures Prepared by Magnetron Plasma Sputtering", *Silicon*, 10(4) (2018) 1411-1418.
[35] E.A. Al-Oubidy and F.J. Al-Maliki, "Effect of Gas Mixing Ratio on Energy Band Gap of Mixed-Phase Titanium Dioxide Nanostructures Prepared by Reactive Magnetron Sputtering Technique", *Iraqi J. Appl. Phys.*, 14(4) (2018) 19-23.
[36] A.M. Hameed and M.A. Hameed, "Highly-Pure Nanostructured Metal Oxide Multilayer Structure Prepared by DC Reactive Magnetron Sputtering Technique", *Iraqi J. Appl. Phys.*, 18(4) (2022) 9-14.

[37] R. Darwesh et al., "Improved radiation shielding properties of epoxy resin composites using Sb_2O_3 and Al_2O_3 nanoparticles additives", *Annals Nucl. Ener.*, 200 (2024) 110385.
[38] G. Angarita et al., "Synthesis of alumina thin films using reactive magnetron sputtering method", *IOP Conf. Ser.: J. Phys.*, 850 (2017) 012022.
[39] M.K. Lambert et al., "Physical properties of γ–Al_2O_3 nanostructures prepared by high-temperature casting", *Mater. Eng. Technol.*, 25(1) (2020) 33-42.
[40] N. Zaim and O. Bayhatun, "A Study on the Gamma-Ray Attenuation Coefficients of Al_2O_3 and $Al_2O_3.TiO_2$ Compounds", Süleyman Demirel University Journal of Natural and Applied Sciences, 22 (2018) 312-318.
[41] G. Zhou et al., "Deposition of nanostructured crystalline alumina thin film by twin targets reactive high power impulse magnetron sputtering", *Appl. Surf. Sci.*, 455 (2018) 310-317.
[42] X. Zheng et al., "Microstructure and electrical contact behavior of Al_2O_3–Cu/30W3SiC(0.5Y_2O_3) composites", *J. Mater. Res. Technol.*, 22 (2023) 2158-2173.

 ISSN (print) 2958-8960 (online) 3006-6042 Printed in IRAQ